

~~CONFIDENTIAL~~Copy 5
RM L52F05

NACA RM L52F05

NACA FOR REFERENCE

NOT TO BE TAKEN FROM

RESEARCH MEMORANDUM

LONGITUDINAL STABILITY, TRIM, AND DRAG CHARACTERISTICS
OF A ROCKET-PROPELLED MODEL OF AN AIRPLANE
CONFIGURATION HAVING A 45° SWEPTBACK
WING AND AN UNSWEPT HORIZONTAL TAIL

By James H. Parks and Alan B. Kehlet

Langley Aeronautical Laboratory
Langley Field, Va.

CLASSIFICATION CANCELLEDAuthority NACA Res. 665 Date 6/12/52RN 102By 7777 6/27/52 See _____

CLASSIFIED DOCUMENT

This material contains information affecting the National Defense of the United States within the meaning of the espionage laws, Title 18, U.S.C., Secs. 793 and 794, the transmission or revelation of which in any manner to an unauthorized person is prohibited by law.

**NATIONAL ADVISORY COMMITTEE
FOR AERONAUTICS**

WASHINGTON
August 12, 1952

CONFIDENTIAL



NATIONAL ADVISORY COMMITTEE FOR AERONAUTICS

RESEARCH MEMORANDUM

LONGITUDINAL STABILITY, TRIM, AND DRAG CHARACTERISTICS

OF A ROCKET-PROPELLED MODEL OF AN AIRPLANE

CONFIGURATION HAVING A 45° SWEPTBACK

WING AND AN UNSWEPT HORIZONTAL TAIL

By James H. Parks and Alan B. Kehlet

SUMMARY


A free-flight investigation was made of the longitudinal stability, trim, and drag of a rocket-propelled airplane model at low lift coefficients at a range of Mach numbers from 0.63 to 1.16. The configuration included a wing and horizontal tail of aspect ratio 4 and thickness ratio in the streamwise direction of 6 percent. The quarter-chord line of the wing was sweptback 45° , whereas the tail was unswept and fixed at 2° incidence, trailing edge down. The center of gravity was located at zero percent of the mean aerodynamic chord. Oscillations induced by pulse rockets were used to obtain stability data.

The lift-curve slopes were linear over the range tested and reached a maximum value of 0.096 at $M = 0.91$. Calculations based on structural influence coefficients obtained from static tests indicate appreciable losses in lifting ability especially at the higher Mach numbers. The configuration exhibited a high degree of stability and stable damping characteristics over the speed range investigated.

A smooth nose-up trim change of low magnitude occurs near $M = 0.90$. The drag coefficient at trim lift increases from a subsonic value of 0.021 to 0.055 near $M = 1.10$.

INTRODUCTION

A general research program has been initiated by the National Advisory Committee for Aeronautics to determine, by means of rocket-propelled models in free flight, the effect of various empennage designs on the transonic longitudinal stability, trim, and drag characteristics



of complete airplane configurations. Presented herein are the results from one of the transonic models having a conventional empennage arrangement with an unswept horizontal tail fixed at 2° incidence, trailing edge down, and mounted on a 45° sweptback vertical tail. The wing was sweptback 45° with an aspect ratio of 4 and thickness ratio of 6 percent in the streamwise direction.

Longitudinal stability, trim, and drag were obtained from an analysis of continuous telemeter records and of short-period oscillations induced by vertically thrusting pulse rockets.

The model was tested at the Pilotless Aircraft Research Station at Wallops Island, Va.

SYMBOLS

b_e	exposed span, ft
\bar{c}	mean aerodynamic chord, ft
g	gravitational acceleration, ft/sec ²
p	static pressure, lb/sq ft
q	dynamic pressure, $\frac{\gamma}{2} \rho M^2$, lb/sq ft
y	increment of exposed span, ft
K	ratio of lift-curve slope of a rigid wing to that of present wing
K_y	radius of gyration about y-axis, ft
t	time, sec
L	unit load, lb
M	Mach number
P	period of the short-period oscillations, sec
R	Reynolds number, based on \bar{c}
S	wing area, sq ft

V	velocity, ft/sec
W	weight of model, lb
I_y	moment of inertia about the y-axis, slug-ft ²
$T_{1/2}$	time to damp to one-half amplitude, sec
a_n/g	normal accelerometer reading, positive up
a_l/g	longitudinal accelerometer reading, positive forward
α	angle of attack, deg
δ_0	horizontal tail deflection for zero angle of attack
γ	ratio of specific heats, 1.4
θ	angle of pitching, radians
θ_t	angle of twist, radians; leading edge positive up
C_N	normal force coefficient, $(W/S)(1/q)(a_n/g)$
C_C	chord force coefficient, $(W/S)(1/q)(-a_l/g)$
C_L	lift coefficient, $C_N \cos \alpha - C_C \sin \alpha$
C_D	drag coefficient, $-C_C \cos \alpha - C_N \sin \alpha$
C_m	pitching-moment coefficient
C_{m_0}	pitching-moment coefficient at zero angle of attack

Subscripts:

$\dot{\alpha}$	$(d\alpha/dt)(\bar{c}/2V)(1/57.3)$
q	$(d\theta/dt)(\bar{c}/2V)$

The symbols α , $\dot{\alpha}$, and q used as subscripts indicate the derivative of the quantity with respect to the subscript; for example, $C_{L_\alpha} = dC_L/d\alpha$.

MODEL AND APPARATUS

Model

A three-view drawing of the model is shown in figure 1(a). The model was constructed mainly from laminated mahogany. Metal plates incorporated in the wing and horizontal tail for additional stiffness and rigidity are shown by the sectional details of figure 1(b).

The wing had an aspect ratio of 4, taper ratio of 0.60, and NACA 65A006 airfoil sections in the streamwise direction with the quarter-chord line sweptback 45° . The horizontal tail had the same geometrical characteristics except the quarter-chord line was unswept. The vertical tail had an aspect ratio of 1.5, taper ratio of 0.50, and NACA 65A008 airfoil sections in the streamwise direction with the quarter-chord line sweptback 45° . The wing had no incidence, whereas the horizontal tail was fixed at 2° incidence, trailing edge down. The center of gravity of the model was located at zero percent of the mean aerodynamic chord.

The fuselage was a parabolic body of revolution of fineness ratio 8.91 which is described fully in reference 1. Fuselage ordinates are given in table I.

Photographs of the model are shown in figure 2. A small metal hook of 1/8-inch steel was attached to the fuselage for boosting purposes. The relative size and location of this hook is shown clearly in figure 2(b). The leading edge of this hook had a sharp wedge section.

Propulsion

The model-booster combination is shown on the launching platform in figure 3. The model was launched at an angle of 60° elevation and was boosted to maximum velocity by an ABL Deacon rocket motor.

Six vertically thrusting pulse rockets were installed in the model (four in the nose section and two in the rearward section). The locations of the pulse rockets are shown in figure 1(c). Each pulse rocket had a total impulse of approximately 8 pound-seconds and a burning time of approximately 0.08 second.

Instrumentation

The model was equipped with an NACA four-channel telemeter which transmitted continuous records of normal and longitudinal accelerations, angle of attack, and total pressure.

The flight path was determined from tracking radar data and atmospheric conditions at altitude were obtained from a radiosonde released immediately after model firing.

DATA ANALYSIS

The technique of data reduction for an analysis of the response of models to abrupt disturbances is described in reference 2 for abrupt elevator deflections. The method applies equally well for models employing pulse rockets. Briefly, however, static longitudinal stability is determined from the periods of the short-period oscillations and dynamic longitudinal stability is determined from the rate of decay of the oscillations. The oscillations occurring during pulse rocket burning are not included in the analysis because the time history of the thrust-forcing function cannot be evaluated accurately.

The trim lift, angle of attack, and drag were determined between pulses directly from the telemetered data and through oscillations by appropriate fairing. The angle-of-attack data were converted to angle of attack of the center of gravity by the methods of reference 3.

A detailed discussion of the accuracy of this type of investigation is found in reference 2. For the particular instrumentation used, the absolute accuracy of C_L and C_D is ± 0.010 and ± 0.003 , respectively, at $M = 1.10$, and ± 0.025 and ± 0.008 , respectively, at $M = 0.70$. The angle of attack is believed to be correct within 0.20° and the Mach number is estimated to be correct within 0.02 at $M = 1.00$.

Since the influence of aeroelasticity on aerodynamic characteristics is important when sweepback is incorporated in a lifting surface, static tests were made to determine the flexibility of the exposed portion of the model wing. Concentrated loads were applied independently at several spanwise stations along the 25-percent and 50-percent chord lines and the resulting angles of twist along the span for each loading condition were determined. Deflection diagrams obtained from these data are presented in figure 4. The variation of dynamic pressure with Mach number is shown in figure 5 for use with structural influence coefficients in the calculation of aeroelastic effects.

RESULTS AND DISCUSSION

The Reynolds numbers of the test are shown in figure 6 as a function of the Mach number. A portion of the flight time-history converted to aerodynamic parameters is shown in figure 7. Seven oscillations, similar to those shown in figure 7, were available for analysis; six induced by pulse rockets between Mach numbers of 0.92 and 0.65 and one at separation ($M = 1.16$) resulting from the differences in trim between the model alone and the model-booster combination. The last pulse rocket fired before the previous oscillation had completed a sufficient number of cycles for the usual stability analysis and thus is included in the lift analysis only. It should be pointed out that all the data analyzed were in the lift-coefficient range of ± 0.20 as shown in figure 8.

Lift

The lift curves obtained are plotted in figure 8. The values of lift-curve slope represented by the faired lines in figure 8 are shown in figure 9. The subsonic value of 0.079 increases abruptly to 0.096 near $M = 0.90$. Near a Mach number of 1.11, the lift-curve slope is 0.061. These values are less than would be obtained from a similar configuration having a rigid wing because of the effects of flexibility mentioned previously.

By using the deflection data of figure 4 in the form of influence coefficients, as suggested in reference 4, a factor by which the flexible wing data may be corrected to the rigid wing case was computed. This factor is shown as a function of Mach number in figure 10. It should be pointed out that this correction is not precise because of the type of data available but rather is presented to indicate the order of magnitude of the losses due to flexibility.

Values of lift-curve slope corrected for the effects of wing flexibility are shown in figure 11; also shown are lift-curve slopes calculated from the wind-tunnel tests of component parts reported in references 5 and 6. The agreement is good except in the region between $M = 0.90$ and $M = 1.00$. The reasons for the discrepancy in this Mach number range are not completely known but similar effects have been noted previously between free-flight and wind-tunnel tests.

Static Longitudinal Stability

Periods of the short-period oscillations are shown as a function of Mach number in figure 12. Since no pulse data were obtained between $M = 0.91$ and $M = 1.11$, a dashed-line fairing is used over this relatively large Mach number increment in the stability analysis plots. These dashed-line fairings are based on unpublished rocket-model data and general considerations of the present test. These data converted to the static stability parameter $C_{m\alpha}$ are shown in figure 13. The configuration is shown to be longitudinally stable throughout the Mach number range for the center-of-gravity location used. In general, the longitudinal stability increased with increasing Mach number. Although some loss occurred between $M = 0.80$ and $M = 0.87$, no severe variations were noted and the loss had been regained at $M = 0.91$.

The degree of longitudinal stability, as indicated by the aerodynamic-center location, is shown in figure 14. At Mach numbers less than 0.87, the shape of the curve is quite similar to the $C_{m\alpha}$ variation.

No attempt was made to isolate the factors contributing to these variations as the influence of wing flexibility was also felt at the tail in the form of changes in downwash. Generally speaking, however, the two major effects of wing flexibility on the configuration stability are in opposite directions; the loss of lift over the wing combined with a forward shift in the wing center of pressure tend to decrease the over-all stability, whereas the moment-producing ability of the tail should increase due to changes in downwash, thereby tending to increase the stability.

Dynamic Longitudinal Stability

The times required for the short-period oscillations to damp to one-half amplitude are shown in figure 15. Damping factors corresponding to these time increments are shown in figure 16. The damping is stable over the Mach number range tested.

Although the total damping factor decreases from approximately 60 at high subsonic Mach numbers to 48 at $M = 1.11$, the damping-moment derivative remains essentially the same, approximately 25. No attempt was made to isolate the variables contributing to the damping caused by the effects of wing flexibility, but apparently the moment-producing ability of the tail increased, whereas the over-all lifting ability, supplied mainly by the wing, decreased with increasing Mach number.

It should be pointed out that a mass-distribution term K_y/\bar{c} was included in the total damping factor. For the present tests, $K_y/\bar{c} = 1.89$. The importance of this term in comparing the present results with the two-degree-of-freedom damping characteristics of configurations with different mass distributions is discussed fully in reference 7.

Longitudinal Trim

The trim lift coefficients for the configuration through the Mach number range are shown in figure 17(a). The shape of the trim curve agrees with the results of reference 8. The fact remains that a pulse rocket fired during the transonic trim change may obscure the exact nature of the variation, but the transition from subsonic to supersonic flight appears to introduce a smooth nose-up change in trim with the trim lift coefficient increasing from 0 at $M = 0.85$ to 0.04 at $M = 0.95$.

Angles of attack corresponding to these trim lift coefficients are shown in figure 17(b). Although the changes in lift-curve slope are reflected in these data, no unusual variations were noted.

By reasonably assuming C_m to vary linearly with C_L (from basic oscillations), a trim curve for a center-of-gravity location at $\bar{c}/4$ was computed and is shown in figure 17(a). The decrease in stability amplifies the magnitude of the trim change but the shape of the trim curve remained essentially the same.

On a similar basis, the trim angles of attack were used to determine the pitching-moment coefficient at zero angle of attack. These values are shown in figure 18. As might be expected from the data presented previously, these pitching-moment coefficients increased with increasing Mach number with the most abrupt change in the region of $M = 0.90$.

It is interesting to note that if the horizontal tail is considered as an all-movable control, zero angle of attack could be maintained throughout the Mach number range with little control movement as shown in figure 19. These values were computed from the relationship $\delta_0 = C_{m_0}/C_{m_\delta}$ where C_{m_δ} is from the wind-tunnel data of reference 5.

The variations in C_{m_0} and δ_0 are believed to be independent of the wing and primarily due to Mach number effects on the down flow over the horizontal tail induced by the convergence of the rearward part of the fuselage from the subsequent considerations. The

wing-fuselage combination is symmetrical about the longitudinal axis and no downwash from the wing should exist at zero angle of attack. The contribution of the empennage drag to the zero-lift pitching-moment coefficient is calculated to be relatively small, 0.003 at $M = 0.70$ and 0.012 at $M = 1.10$. The same effects are shown in the more complete data of reference 9 wherein similar total changes of approximately 0.06 in C_{m_0} and 1° in horizontal tail deflections were noted.

Drag

The drag coefficients at trim lift coefficients throughout the test Mach number range are shown in figure 20. The subsonic value of 0.021 increasing to 0.055 at $M = 1.11$ with the most abrupt increase near $M = 0.95$ is of the order of magnitude which might be expected from the geometry of the configuration. The reasons for the hook and subsequent increase in abruptness of the drag rise near $M = 0.94$ is believed due to pressure changes on the rear fuselage and have been noted previously on similar configurations (ref. 10).

Minimum drag values are also shown in figure 20 and, except near $M = 1.11$, the trim lift had no appreciable effect on the drag coefficient. The lift-coefficient range of the transient oscillations was not great enough to determine the effect of lift on drag with any degree of accuracy.

CONCLUSIONS

From the flight tests at low lift coefficients of a rocket-propelled model of an airplane configuration having a 45° sweptback wing and an unswept horizontal tail with 2° incidence, the following conclusions may be drawn:

1. The lift-curve slopes were linear over the ranges tested with a maximum value of 0.096 at $M = 0.91$. Calculations based on static loading data indicated that losses in lift due to wing flexibility occurred over the entire speed range with the magnitude of the losses increasing with increasing Mach number.

2. The aerodynamic-center location remained near 60 percent \bar{c} at subsonic Mach numbers. At $M = 1.11$, however, the aerodynamic center location had moved rearward to 88 percent \bar{c} .

3. The configuration exhibited stable damping characteristics over the Mach number range.

4. A longitudinal transonic trim change occurred near $M = 0.90$ in a nose-up direction. The change in trim was smooth and of small magnitude.

5. The drag coefficient at trim lift increased from 0.021 at subsonic speeds to 0.055 at supersonic speeds.

Langley Aeronautical Laboratory
National Advisory Committee for Aeronautics
Langley Field, Va.

REFERENCES

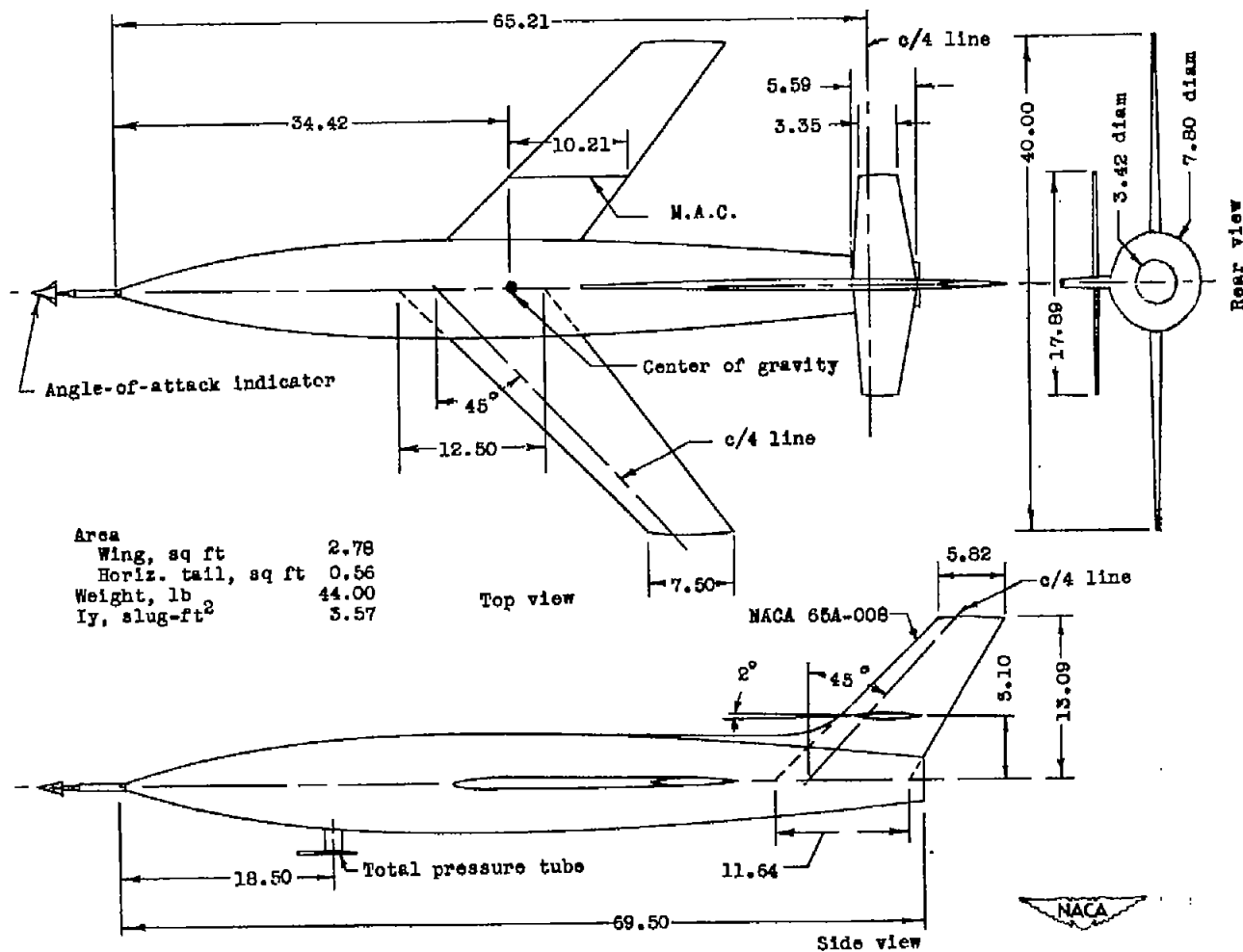
1. Hart, Roger G., and Katz, Ellis R.: Flight Investigations at High-Subsonic, Transonic, and Supersonic Speeds to Determine Zero-Lift Drag of Fin-Stabilized Bodies of Revolution Having Fineness Ratios of 12.5, 8.91, and 6.04 and Varying Positions of Maximum Diameter. NACA RM L9I30, 1949.
2. Gillis, Clarence L., Peck, Robert F., and Vitale, A. James: Preliminary Results From a Free-Flight Investigation at Transonic and Supersonic Speeds of the Longitudinal Stability and Control Characteristics of an Airplane Configuration With a Thin Straight Wing of Aspect Ratio 3. NACA RM L9K25a, 1950.
3. Mitchell, Jesse L., and Peck, Robert F.: An NACA Vane-Type Angle-of-Attack Indicator for Use at Subsonic and Supersonic Speeds. NACA RM L9F28a, 1949.
4. Diederich, Franklin W.: Calculation of the Aerodynamic Loading of Swept and Unswept Flexible Wings of Arbitrary Stiffness. NACA Rep. 1000, 1950. (Supersedes NACA TN 1876.)
5. Donlan, Charles J., Myers, Boyd C., II, and Mattson, Axel T.: A Comparison of the Aerodynamic Characteristics at Transonic Speeds of Four Wing-Fuselage Configurations as Determined From Different Test Techniques. NACA RM L50H02, 1950.
6. Osborne, Robert S.: A Transonic-Wing Investigation in the Langley 8-Foot High-Speed Tunnel at High Subsonic Mach Numbers and at a Mach Number of 1.2. Wing-Fuselage Configuration Having a Wing of 45° Sweepback, Aspect Ratio 4, Taper Ratio 0.6, and NACA 65A006 Airfoil Section. NACA RM L50H08, 1950.
7. Mitchell, Jesse L.: The Static and Dynamic Longitudinal Stability Characteristics of Some Supersonic Aircraft Configurations. NACA RM L52A10a, 1952.
8. Parks, James H., and Mitchell, Jesse L.: Longitudinal Trim and Drag Characteristics of Rocket-Propelled Models Representing Two Airplane Configurations. NACA RM L9L22, 1950.
9. Gillis, Clarence L., and Vitale, A. James: Wing-On and Wing-Off Longitudinal Characteristics of an Airplane Configuration Having a Thin Unswept Tapered Wing of Aspect Ratio 3, As Obtained From Rocket-Propelled Models at Mach Numbers From 0.8 to 1.4. NACA RM L50K16, 1951.

10. Morrow, John D., and Nelson, Robert L.: Large-Scale Flight Measurements of Zero-Lift Drag of 10 Wing-Body Configurations at Mach Numbers From 0.8 to 1.6. NACA RM L52D18a, 1952.

TABLE I
FUSELAGE ORDINATES

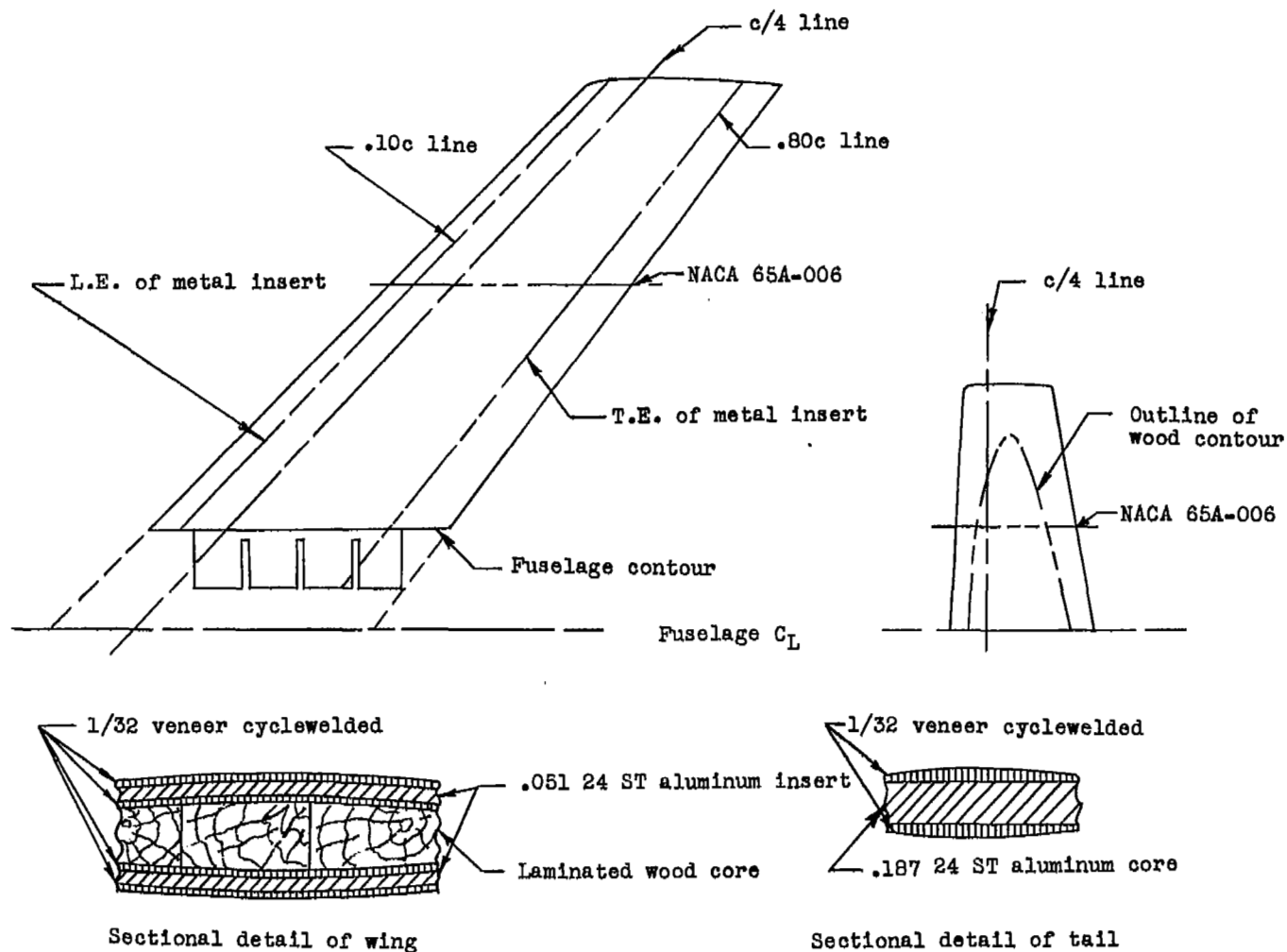
Station (in.)	Diameter (in.)
0	0
3	1.60
6	3.00
9	4.24
12	5.28
15	6.14
18	6.84
21	7.34
24	7.66
27.8	7.80
30	7.78
33	7.74
36	7.64
39	7.48
42	7.30
45	7.06
48	6.78
51	6.44
54	6.08
57	5.66
60	5.18
63	4.68
66	4.12
69.5	3.42





(a) General arrangement of model.

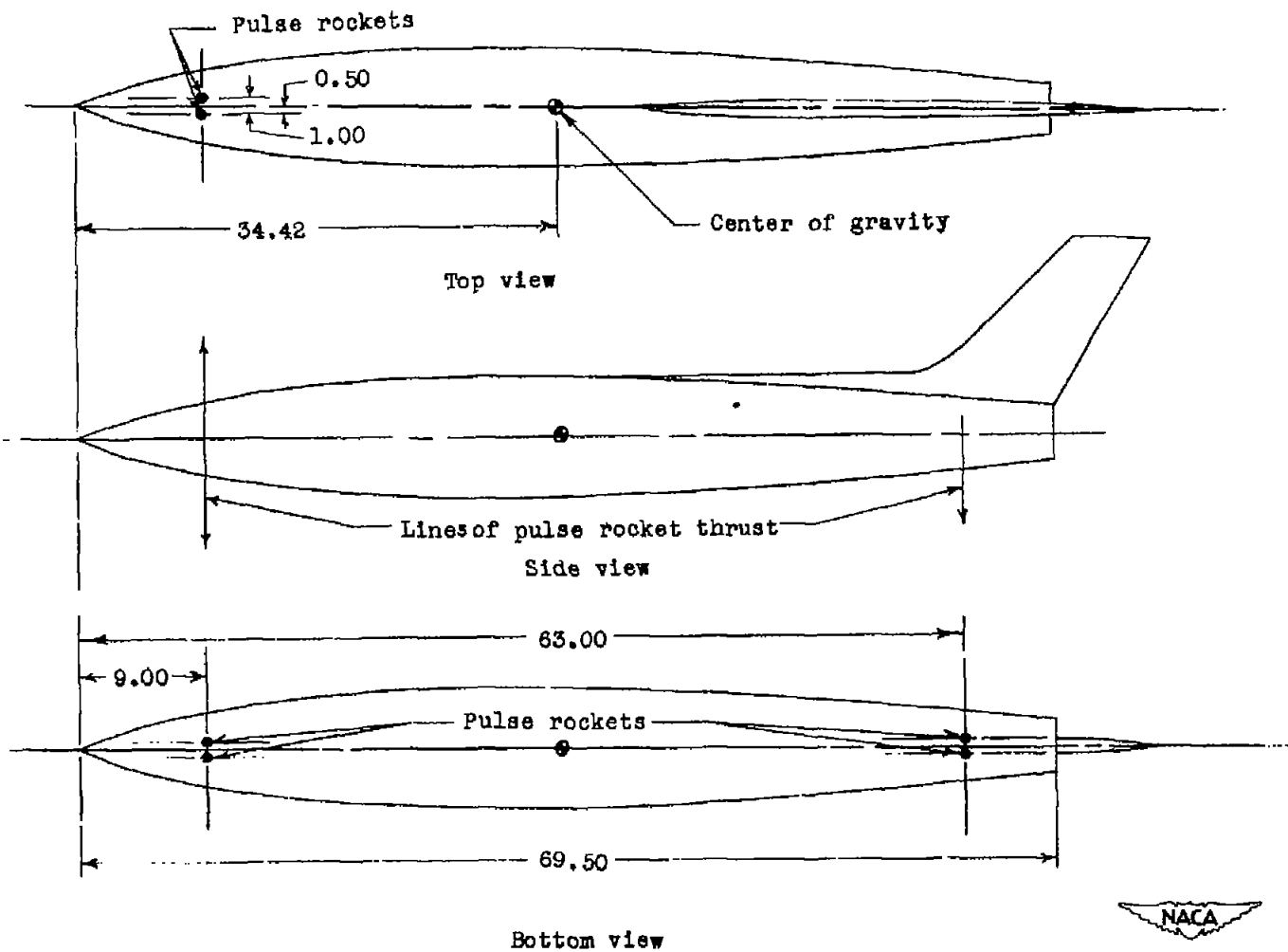
Figure 1.- Arrangement and construction details of model. All dimensions are in inches.



(b) Details of wing and tail construction.

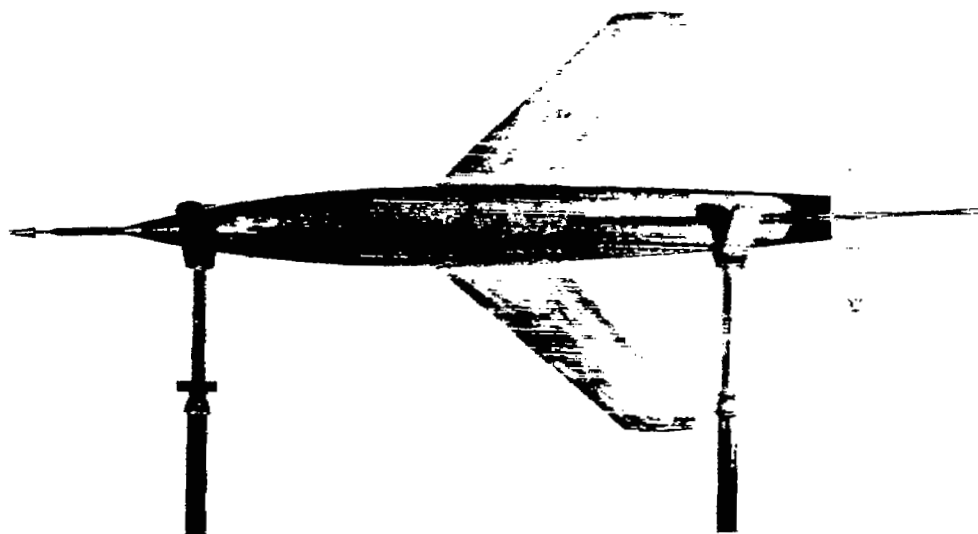
Figure 1.- Continued.





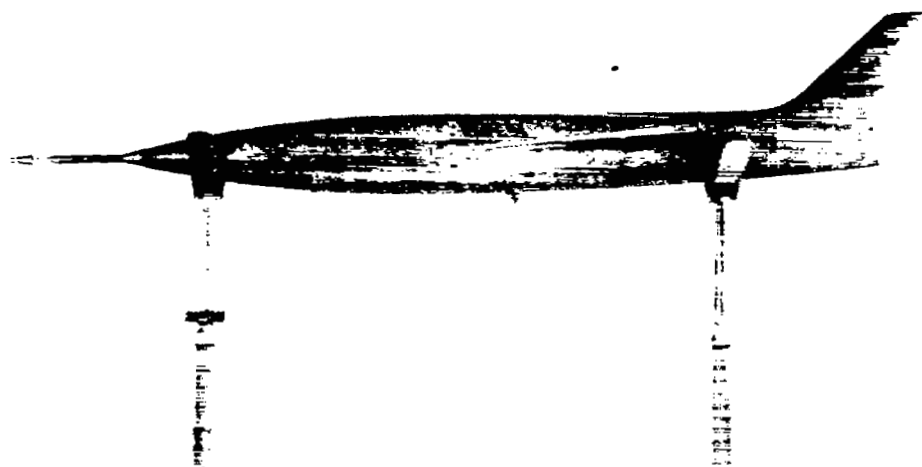
(c) Arrangement of the pulse rockets in the fuselage.

Figure 1.- Concluded.



(a) Top view.

NACA
L-72331.1



(b) Side view.

NACA
L-72332.1

Figure 2.- Photographs of the model.

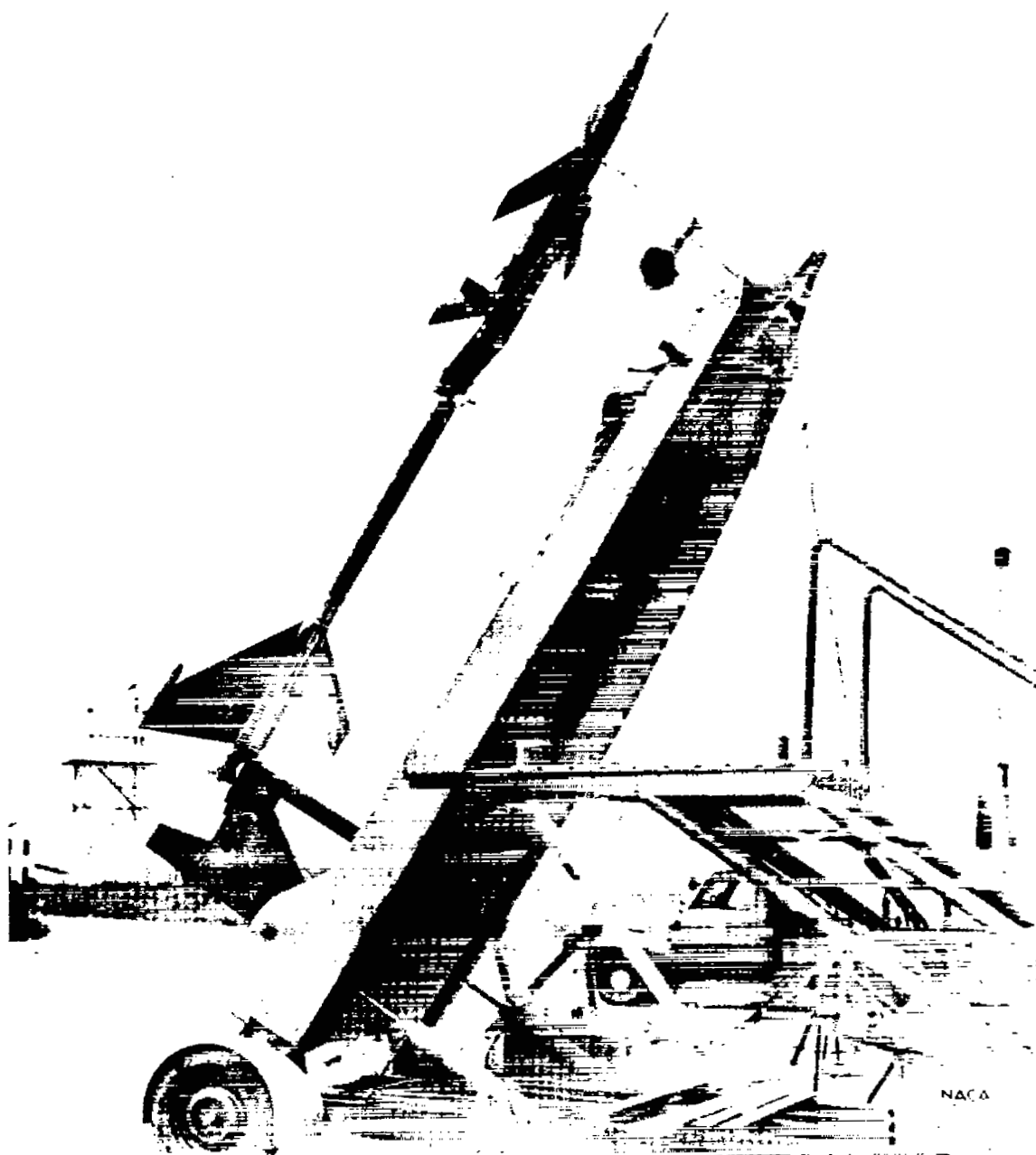
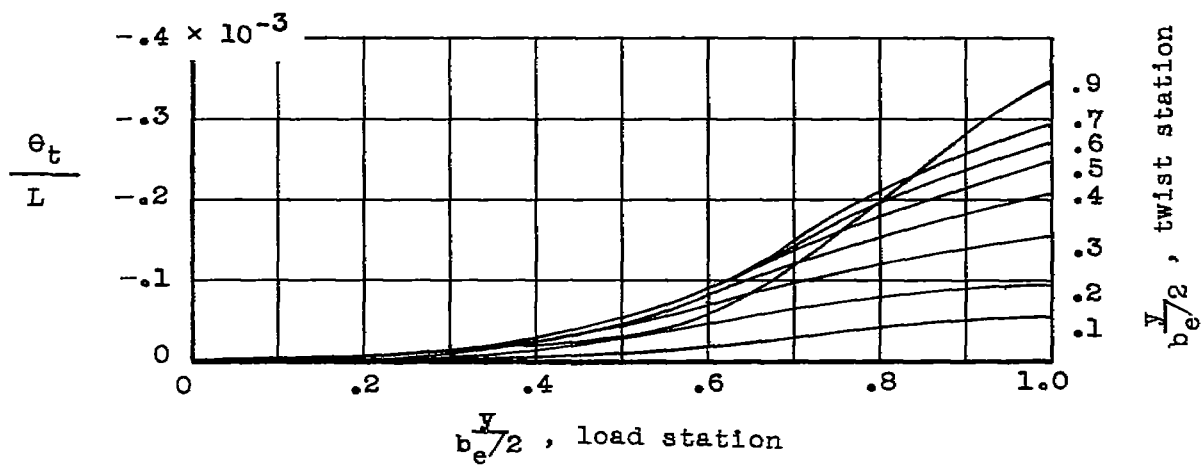
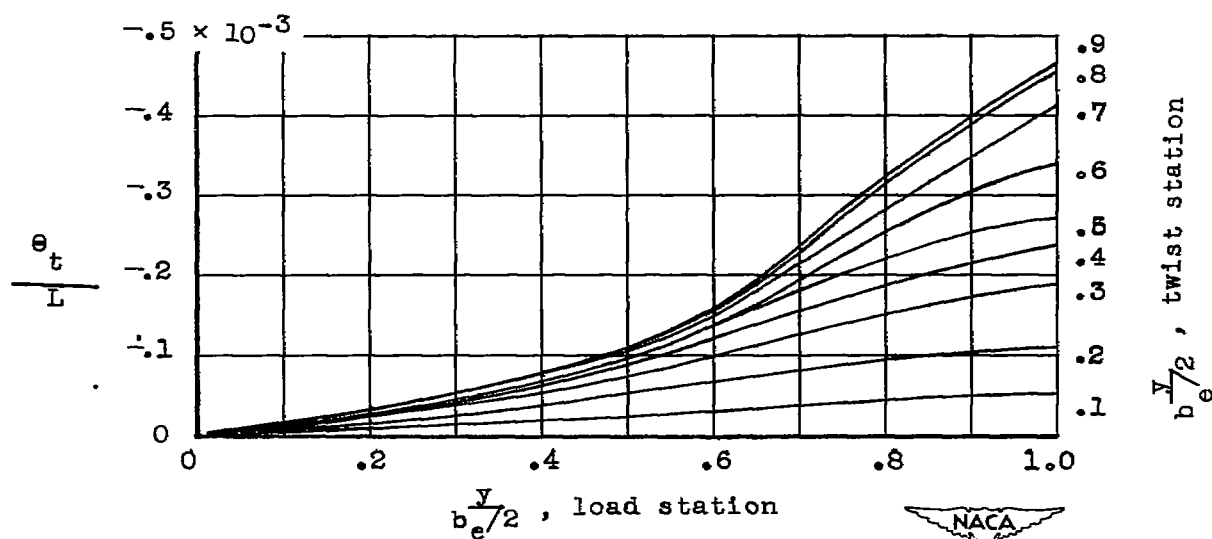


Figure 3.- Photograph of the model-booster combination on the launching platform.



(a) Loads at 0.25 chord line.



(b) Loads at 0.50 chord line.

Figure 4.- Deflection diagrams obtained from static loading tests on the exposed model wing.

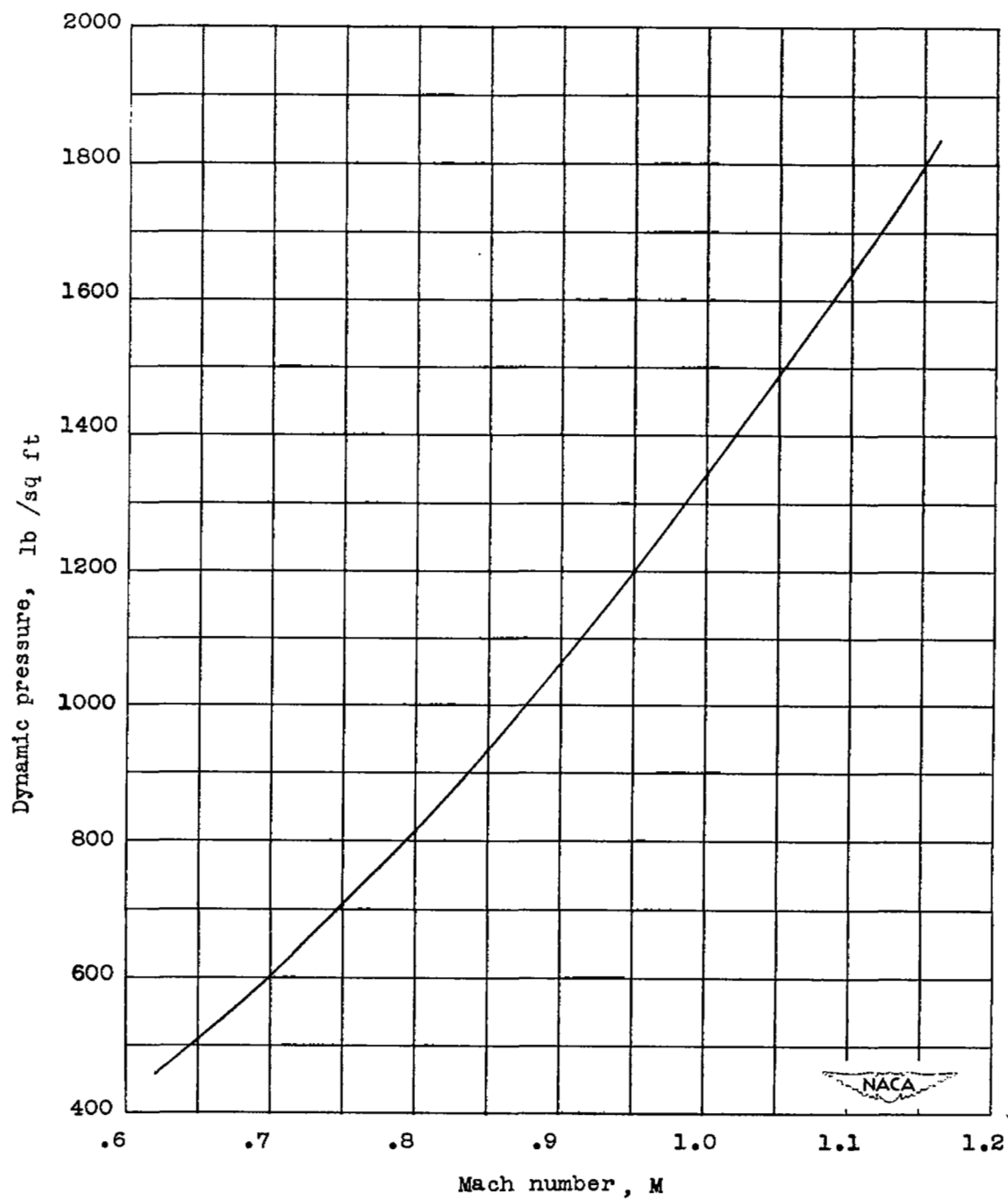


Figure 5.- Variation of dynamic pressure with Mach number.

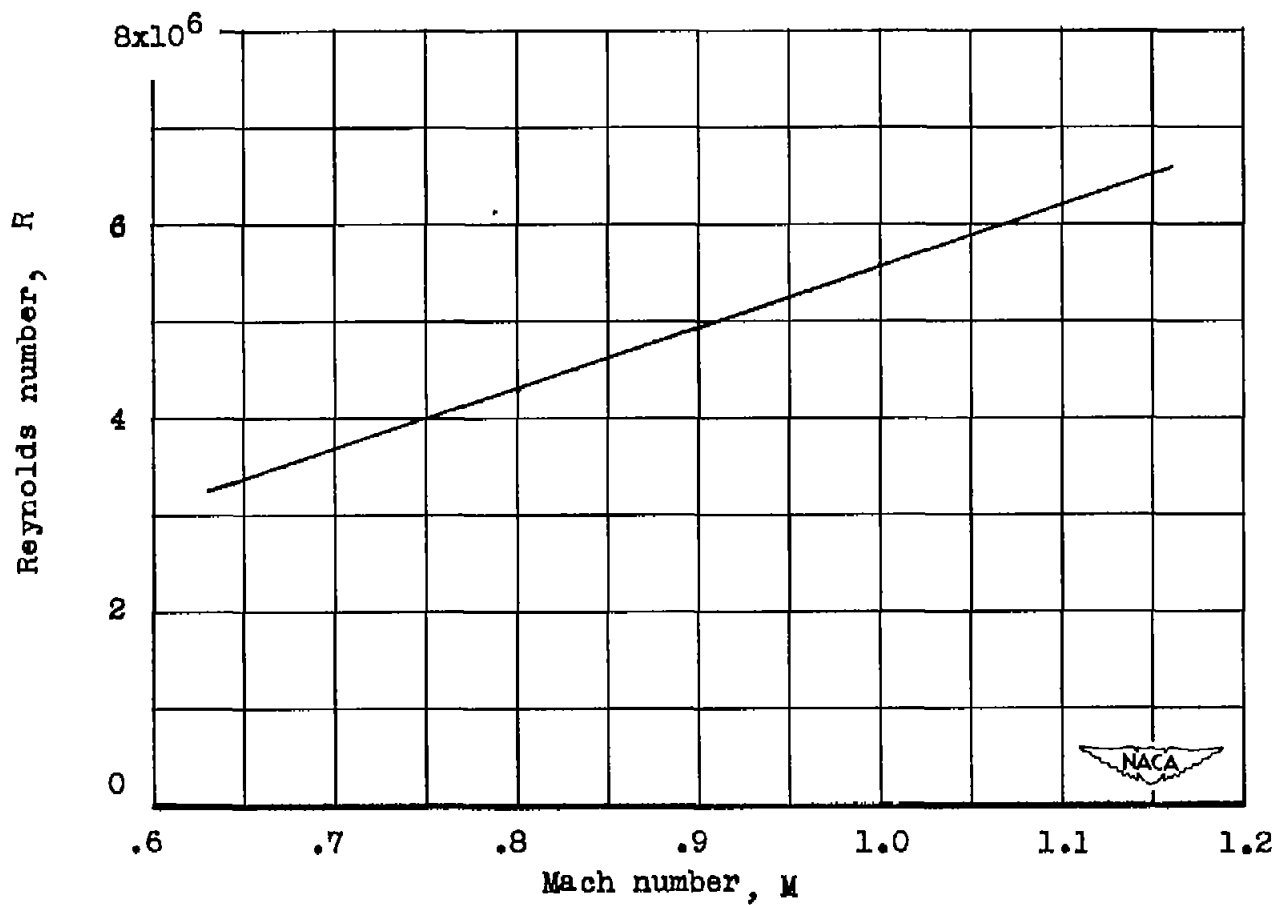


Figure 6.- Variation of Reynolds number with Mach number.

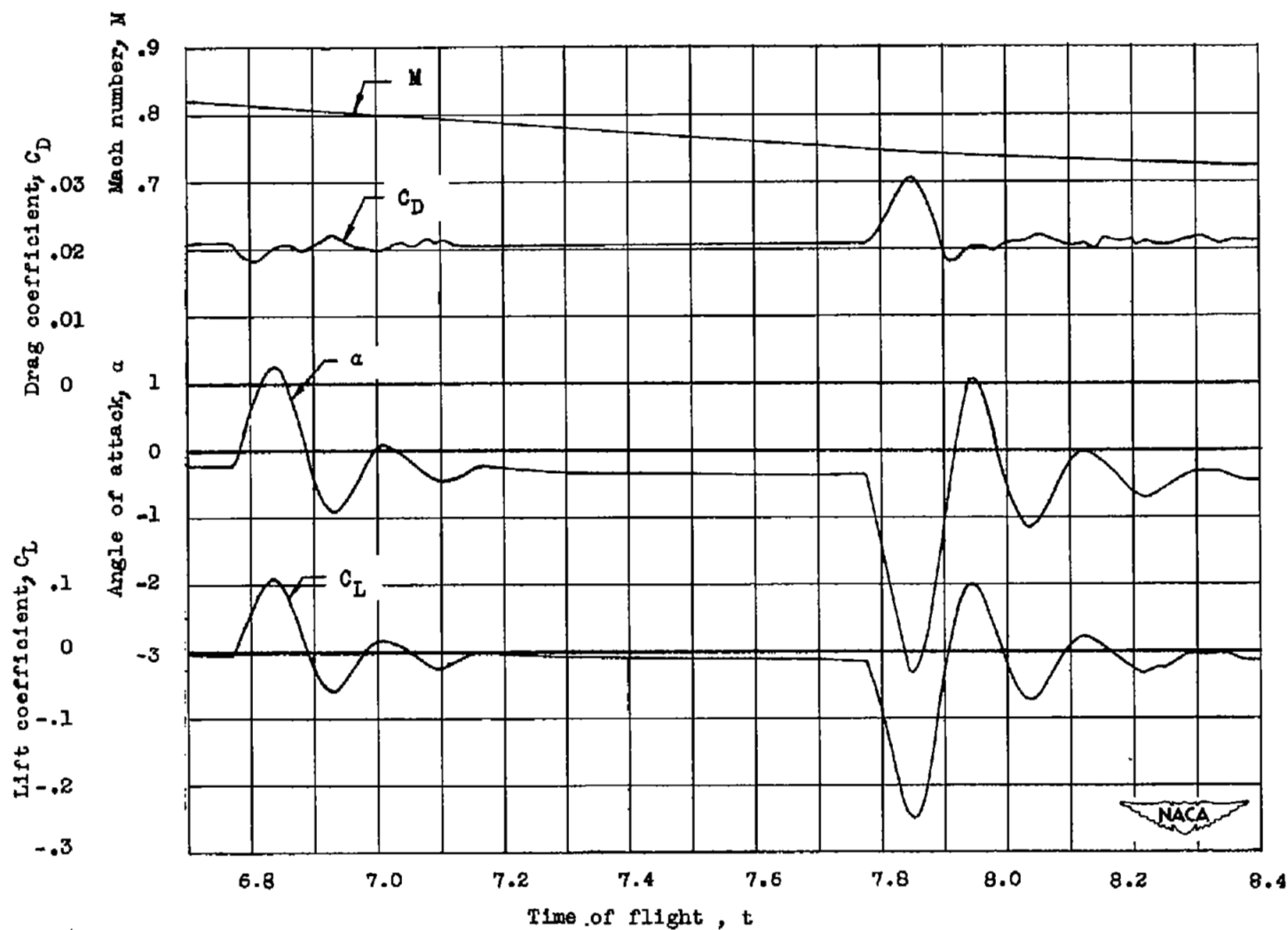


Figure 7.- Portion of the time history of the flight converted to aerodynamic coefficients.

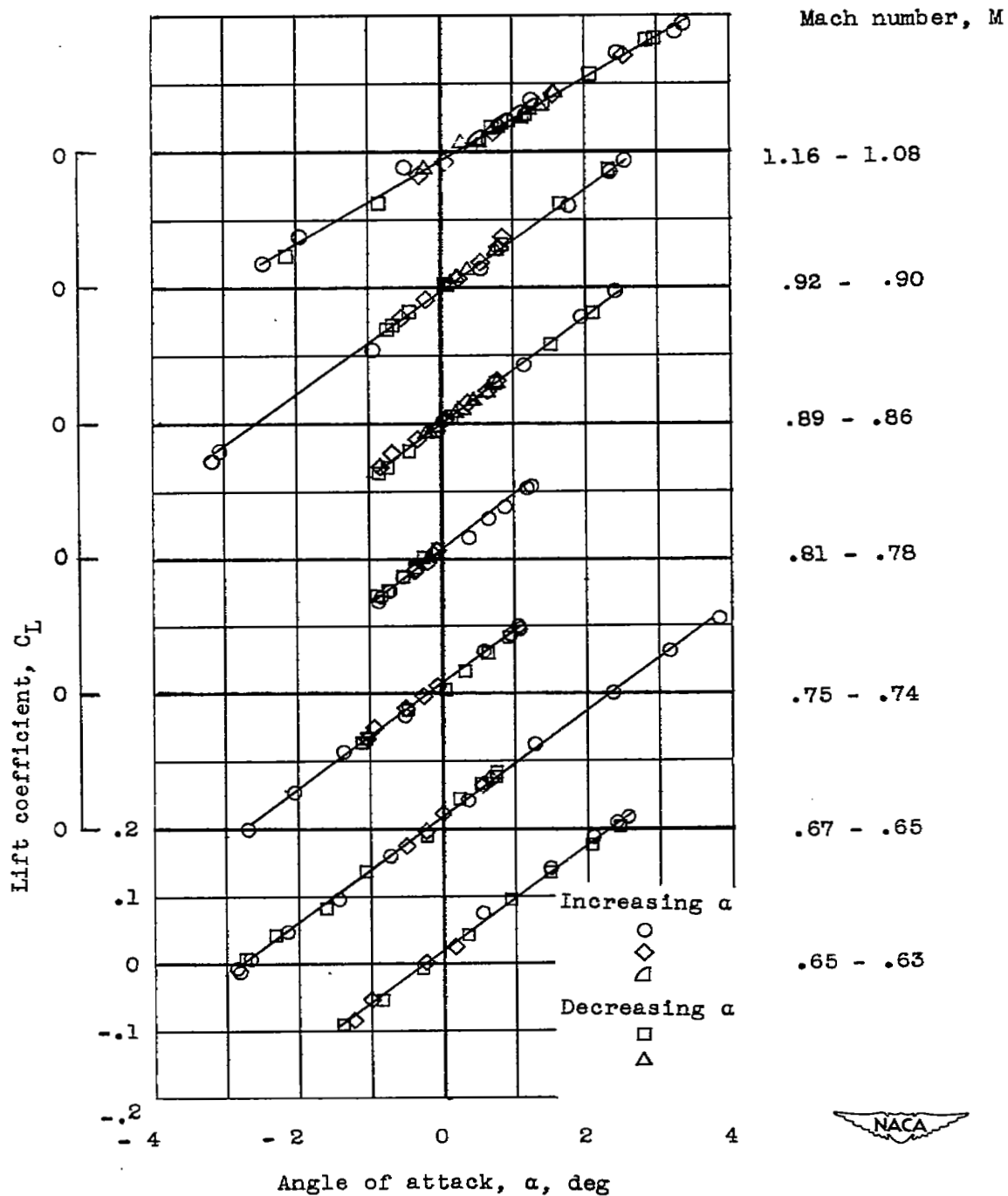


Figure 8.- Lift-curve data obtained from the short period oscillations.

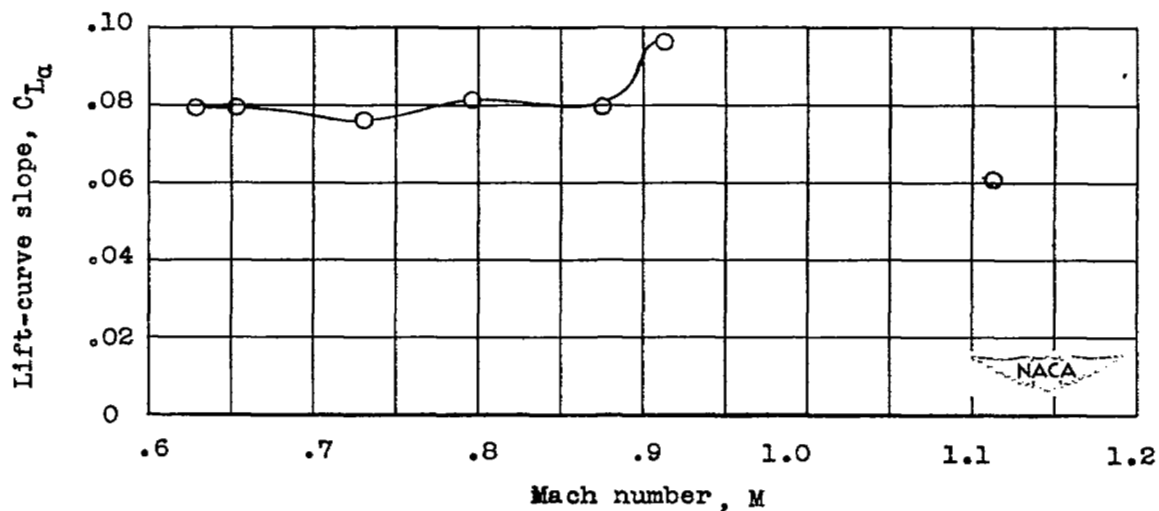


Figure 9.- Variation of the lift-curve slope with Mach number.

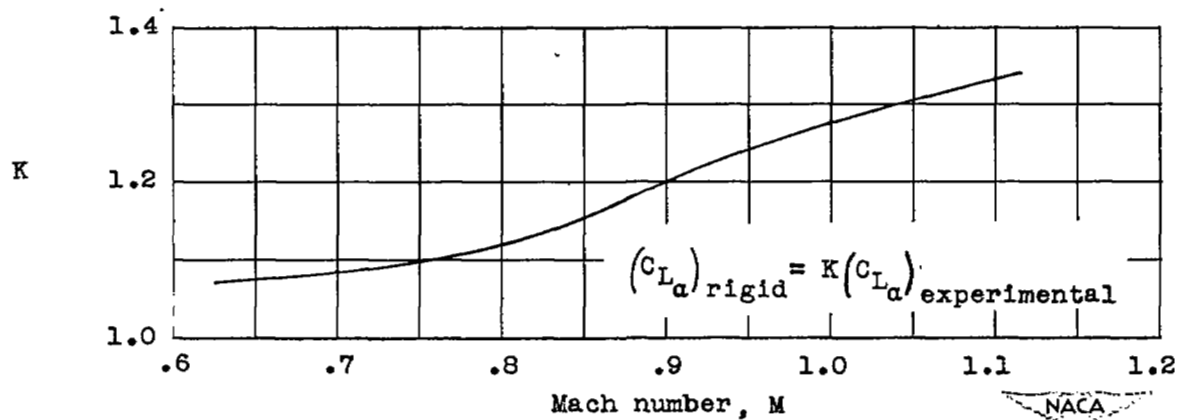


Figure 10.- Factors for converting the flexible wing lift-curve slopes to the rigid case.

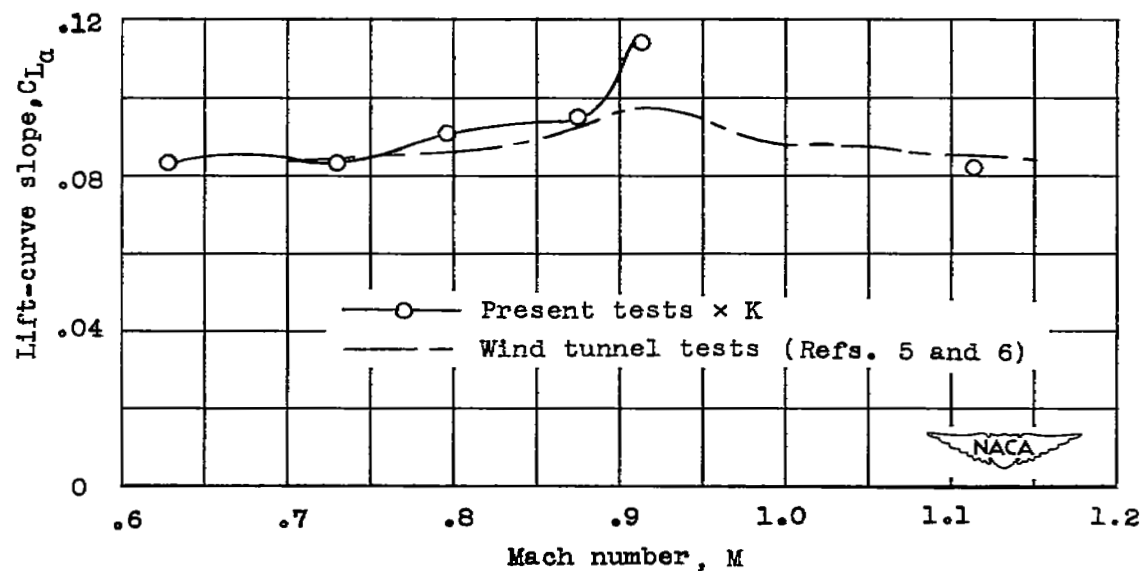


Figure 11.- Comparison of lift-curve slopes from two techniques with the effects of aeroelasticity considered.

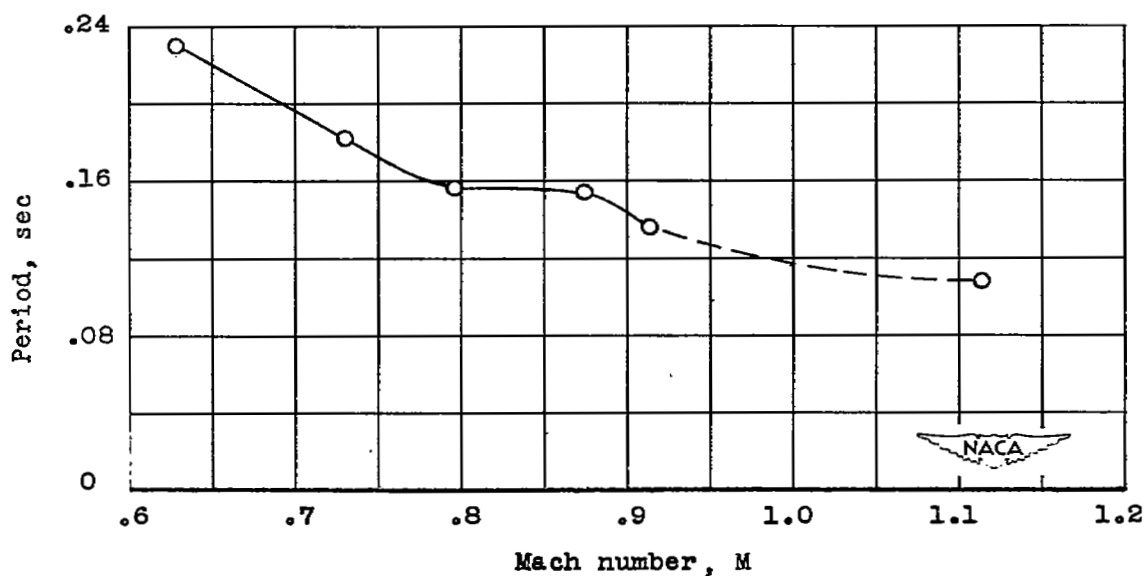


Figure 12.- Variation of the periods of the transient oscillations with Mach number.

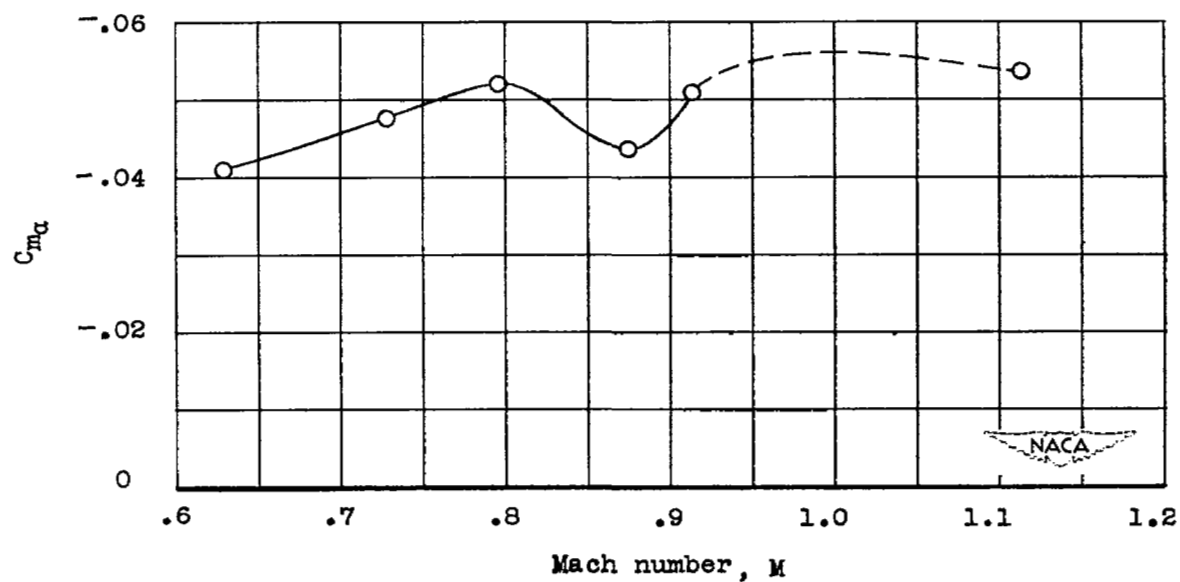


Figure 13.- Variation of the static stability parameter with Mach number.

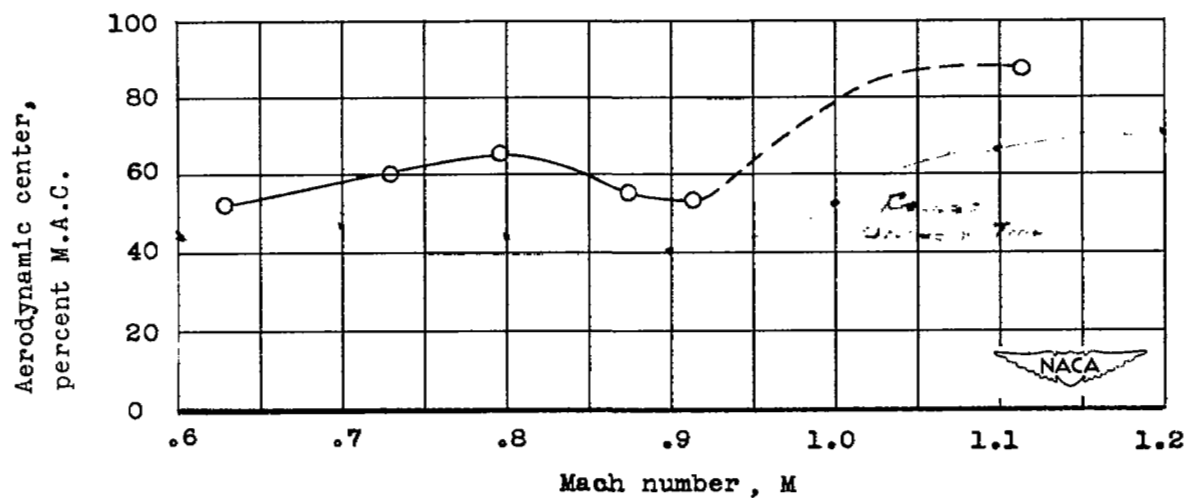


Figure 14.- Variation of the aerodynamic-center location with Mach number.

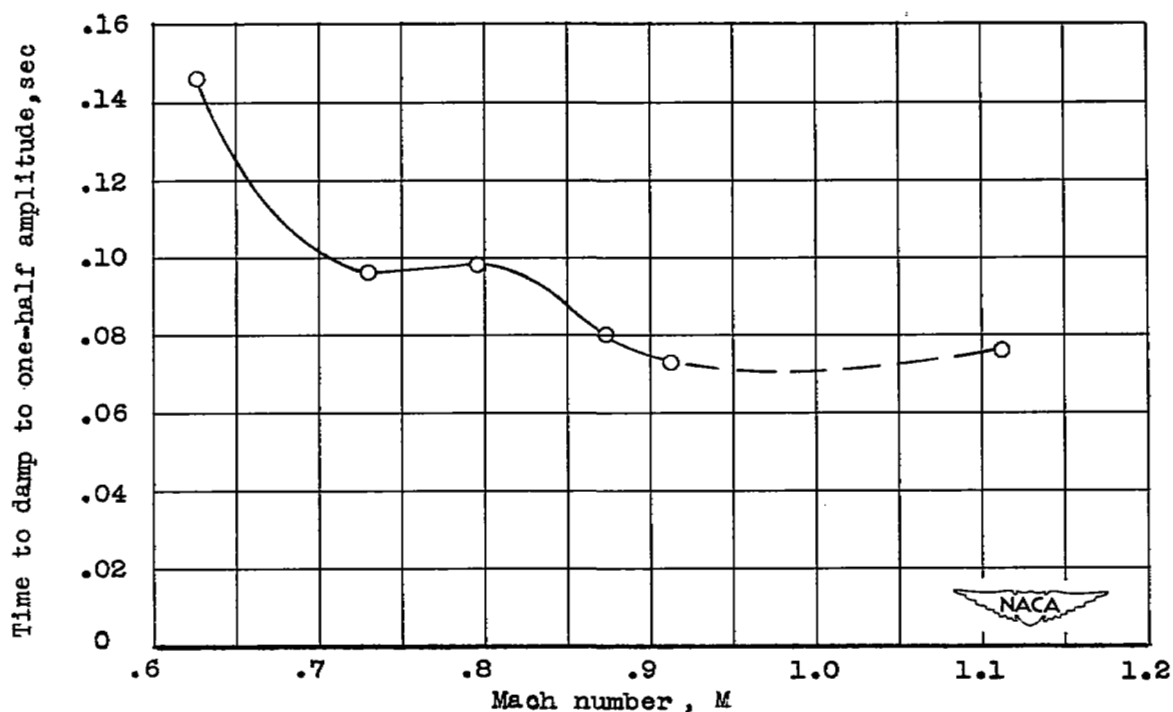


Figure 15.- Times required for the short period oscillations to damp to one-half amplitude as a function of Mach number.

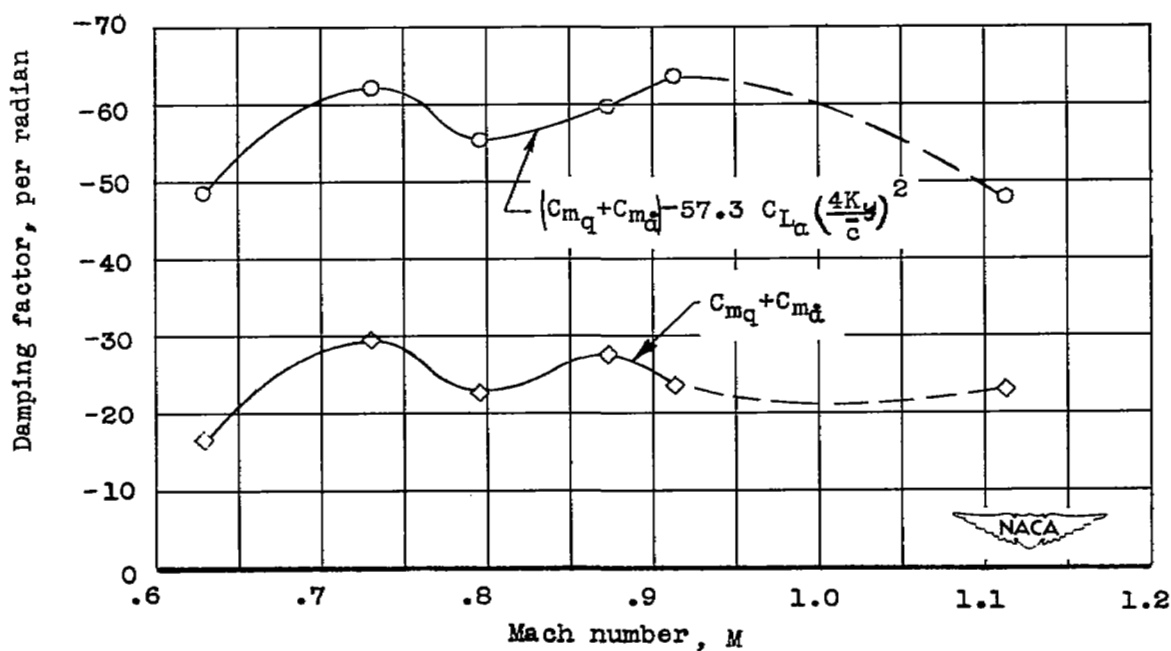
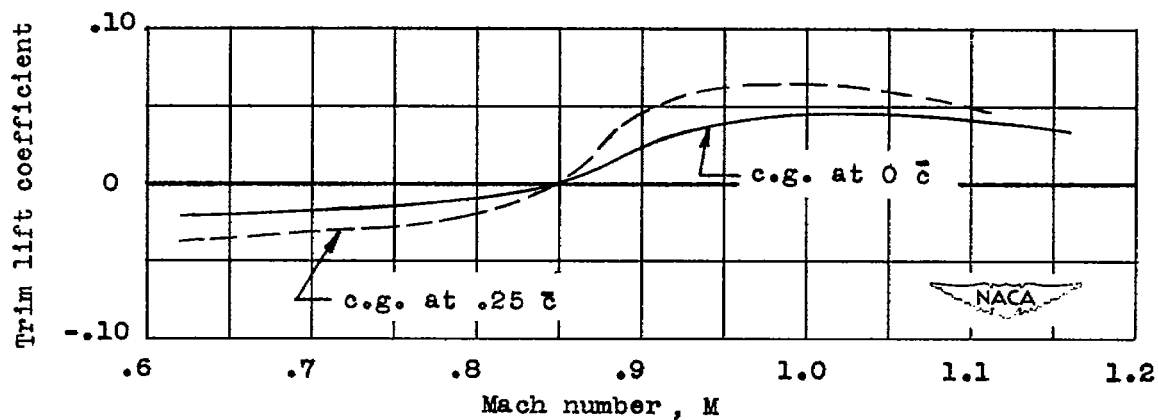
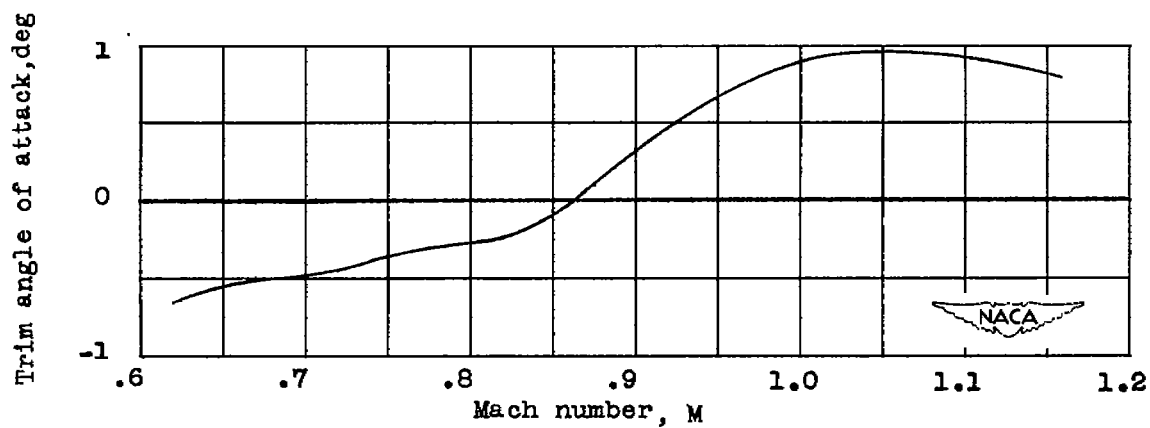


Figure 16.- Variation of damping factors with Mach number.



(a) Lift coefficient.



(b) Angle of attack.

Figure 17.- Longitudinal trim characteristics as a function of Mach number.

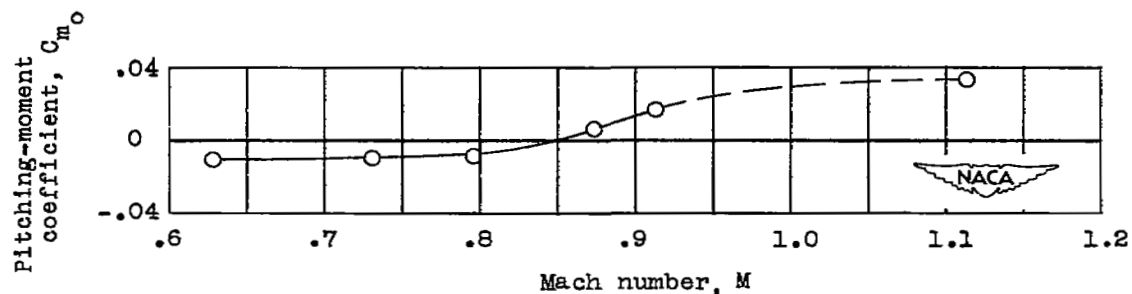


Figure 18.- Variation of the pitching-moment coefficient at zero angle of attack with Mach number.

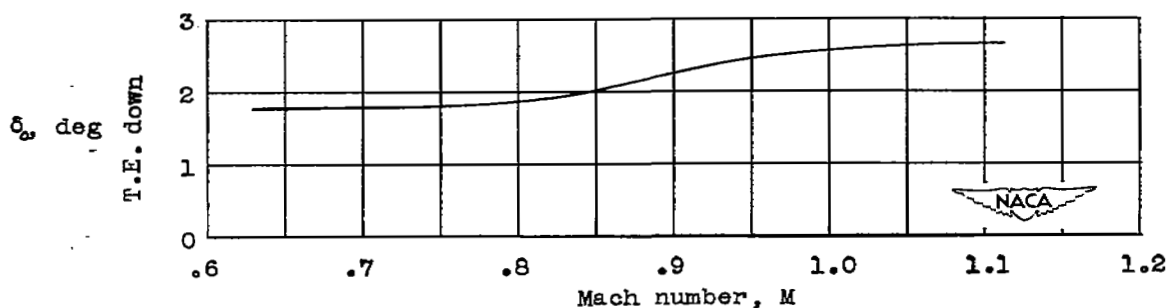


Figure 19.- Horizontal tail deflection required to maintain zero angle of attack (determined by using C_{m0} from ref. 5).

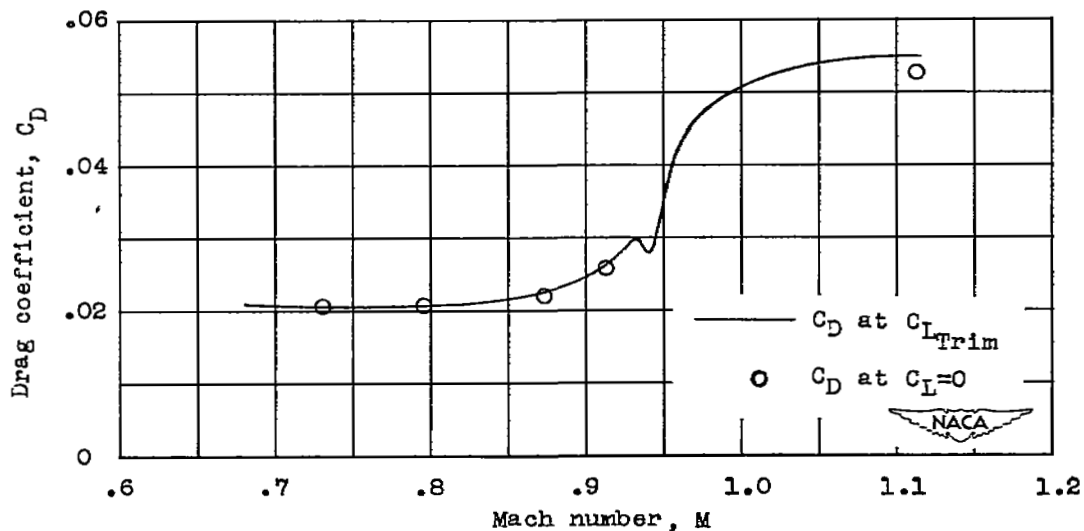


Figure 20.- Variation of drag coefficients with Mach number.

SECURITY INFORMATION

NASA Technical Library



3 1176 01436 4807

